Chemosphere 218 (2019) 83–92

Contents lists available at ScienceDirect

Chemosphere

journal homepage: www.elsevier.com/locate/chemosphere

Transformation pathway and degradation mechanism of methylene blue through β-FeOOH@GO catalyzed photo-Fenton-like system

Shanshan Su [a, b], Yuyang Liu [a, b], Xuemin Liu [a, b], Wei Jin [c], Yaping Zhao [a, b, *]

[a] School of Ecological & Environmental Science, Shanghai Key Laboratory for Urban Ecological Process and Eco-Restoration, East China Normal University, Shanghai 200241, China
[b] Institute of Eco-Chongming, Shanghai 200062, China
[c] School of Environmental Science and Engineering, Tongji University, Shanghai 200071, China

HIGHLIGHTS

- β-FeOOH@GO greatly enhanced Fenton oxidation efficiency.
- $^{\bullet}OH$, $HO_2^{\bullet-}$ and $^1O_2$ radicals were involved this system.
- Degradation intermediates on catalyst surface was identified with TOF-SIMS.
- A series of newly identified intermediates were reported first time.
- Synergistic catalytic mechanism of β-FeOOH@GO was elucidated.

ARTICLE INFO

Article history:
Received 1 September 2018
Received in revised form
22 October 2018
Accepted 14 November 2018
Available online 16 November 2018

Handling Editor: Jun Huang

Keywords:
β-FeOOH
Graphene oxide
Methylene blue
Photo-Fenton-like reaction
Degradation mechanism

ABSTRACT

To enhance the catalytic and separation properties of akaganéite nanoparticles, rice spike-like akaganéite impregnated graphene oxide (β-FeOOH@GO) nanocomposite was fabricated through facile hydrolysis. The apparent first-order decolorization rate of methylene blue (MB) in β-FeOOH@GO catalyzed photo Fenton-like system was 0.6322 min^{-1} about 3 folds that of prinstine β-FeOOH nanoparticles. The degradation intermediates of MB adsorbed on the solid surface of β-FeOOH@GO were comprehensively identified with time of flight-secondary ion mass spectroscopy (TOF-SIMS) for the first time. Newly identified sulfoxide intermediates, sulphone intermediates and desulfurization intermediates and N-demethylaton or dedimethamine intermediates were reported for the first time. The proposed degradation pathway of MB predominantly proceeded with the rupture of phenothiazine rings oxided with $^{\bullet}OH$, $HO_2^{\bullet-}$ and singlet oxygen ($^1O_2$) radicals, which fully extending the reaction pathways proposed in previous work in literature. The enhanced catalytic activity of β-FeOOH@GO was ascribed to the formation of heterojunctions confirmed by the presence of Fe—O—C chemical bonds through X-ray photoelectron spectroscopy (XPS). The complete elimination of MB and its acute toxicity to Luminous bacteria showed that β-FeOOH@GO would be served as a highly efficient Fenton-like catalyst for treatment of high concentration refractory organic contaminant.

1. Introduction

Advanced oxidation processes (AOPs) have been emerged as one of the most effective methods to degrade refractory organic pollutants (Brillas and Martinez-Huitle, 2015; Chowdhury and Balasubramanian, 2014; Zangeneh et al., 2015). The conventional Fenton reaction involves the generation of highly oxidative and non-selective $^{\bullet}OH$ ($E^0 = 2.80$ V vs NHE) and the less oxidative $O_2^{\bullet-}$ ($E^0 = 1.30$ V vs NHE) (Bossmann et al., 1998) in the mixture of stoichiometric amounts of Fe^{2+} salts and a large excess of H_2O_2 at acidic pH (Bae et al., 2013; Zhang et al., 2002). Fenton-like catalysis would be an optimum alternative by using iron-containing minerals in the elimination of refractory organic pollutants, such as hematite (Fe_2O_3), iron (oxy)hydroxide (FeOOH) (Mazellier and Bolte, 2000), magnetite (Fe_3O_4) (Ruales-Lonfat et al., 2015) and

* Corresponding author. School of Ecological & Environmental Science, Shanghai Key Laboratory for Urban Ecological Process and Eco-Restoration, East China Normal University, Shanghai 200241, China.
E-mail address: ypzhao@des.ecnu.edu.cn (Y. Zhao).

https://doi.org/10.1016/j.chemosphere.2018.11.098
0045-6535/

pyrite (FeS_2) (Bae et al., 2013). However, most of them did not show favorable photocatalytic activity due to their small particles, severe aggregation, loss of catalytic activity and difficult separation.

Compositing technology was reported to greatly improve or enhance the catalytic activity of iron-containing minerals for the purpose of practical application by assembling them with ideal supports. Among most studied iron-containing mineral composites, such as Fe_3O_4-MWCNTs (Hu et al., 2011), Fe_2O_3-ACF (Lan et al., 2015), $FePO_4$-GO (Guo et al., 2015) and $ZnFe_2O_4$–g-C_3N_4 (Yao et al., 2014), the graphene oxide (GO), used as catalysts' support recently, has triggered a revolution in the field of supporting materials. GO can absorb photons in the ultraviolet, visible, and infrared regions because of its zero-band gap energy (Wassei and Kaner, 2013). With unique mono-layered two-dimensional morphology and band gap structure, GO showed excellent electron accepting, storing and transferring ability (Kim et al., 2013). The existence of GO obviously contributes to the adsorption of reactants and the mass transfer to the photoactive centers through the interface (He et al., 2011). The excellent electrical conductivity of GO also contributes to shuttling the captured electrons rapidly to the catalytic active sites or oppressing the photogenerated electron-hole pair recombination. Williams and coauthors demonstrated the photoelectrons generated from TiO_2 transferred to GO leading to improved photocatalytic activity of TiO_2 through the suppression of electron–hole recombination proving GO would be an ideal electron sinks or transfer bridges (Leary and Westwood, 2011; Williams et al., 2008). For example, Qiu and coauthors reported that the commercial Fe_2O_3 exhibited nearly 100% decolorization rate of methyl orange in the photo-Fenton-like reaction the Fe_2O_3/GO aerogel remained around 90% decolorization rate during 10 cycles (Qiu et al., 2015). The existence of graphene oxide enhanced the separation of the photoexcited electron-hole pairs of Fe_2O_3, the mobility of photo-induced carriers and provision of high-surface area for adsorption of dyes (Jia et al., 2013; Li et al., 2014; Song et al., 2012). While with the same GO support, the Fe_2O_3/GO composites showed poor catalytic and recycled property just as that of commercial Fe_2O_3 due to dissolved iron from the catalyst in the same study (Qiu et al., 2015). One of iron oxides, akaganéite (β-FeOOH) has caused great attention in catalysis because of its natural abundance in the environment, catalytic property and biocompatibility. However, β-FeOOH minerals are usually present as fine or ultrafine particles, easy to agglomerate and difficult to be separated from water phase for its nano-size effect. β-FeOOH shows semiconductor property with narrow band gap energy of 2.12 eV and it can effectively harvests the visible light in solar spectrum. But its poor electron-hole pair separation efficiency and short life of photogenic carriers have become a bottleneck for β-FeOOH practical application in photocatalytic field (Ruales-Lonfat et al., 2015). In order to improve light absorption, catalytic efficiency and electron-hole pair separation of β-FeOOH (Espinosa et al., 2015; Guo et al., 2015), β-FeOOH@GO was composited through forced hydrolysis in our previous work and used as environmental adsorbent for fluoride from water (Iiu et al., 2016).

In this study, we want to explore the catalytic performance of β-FeOOH@GO as a Fenton-like catalyst. A representative dyestuffs methylenen blue (MB) was chosen as a model refractory organic pollutant due to its wide application in chemical industry, printing and dyeing, medicine, aquaculture and its carcinogenic effects on living organisms (Banat et al., 1996; Barrios-Ziolo et al., 2015; Rai et al., 2005). The effectiveness, degradation intermediates and possible catalytic degradation mechanism of MB discolorization in β-FeOOH@GO catalyzed photo-Fenton-like system were systematically evaluated.

2. Materials and methods

2.1. Photo-Fenton-like degradation experiments

Catalyst β-FeOOH@GO was synthesized according to our previous work (Iiu et al., 2016), briefly, 2.7 g of $FeCl_3 \cdot 6H_2O$ was added into 100 ml volume of 1000 mg l^{-1} of GO solution followed with magnetic stirring at 80 °C for 4 h. The typical degradation experiment was performed by adding a desired amount of β-FeOOH@GO (0.25 g L^{-1}) and H_2O_2 (1.10 mM) into 400 ml of 40 mg L^{-1} MB solution in a pyrex reactor. The pH was adjusted with 0.1 M HCl or NaOH. The suspension was stirred with a magnetic stirrer at air-conditioned room at 20 °C and irradiated with a 125 W high-pressure mercury UV lamp (Phillips GGY125Z ballast with main wavelength of 365 nm and irradiation intensity of 1.94 mW cm^{-2}). The recycling experiments of β-FeOOH@GO were consecutively carried out with 60 min of dark adsorption followed by 60 min of photo Fenton-like catalytic reaction without any other post treatment. About 5 ml aliquot was withdrawn at predetermined time intervals. All experiments were conducted in triplicate with relative standard deviation less than 5%.

2.2. Analytical methods

MB concentration was measured through UV–Vis spectrophotometer at wavelength of 665 nm. Total dissolved iron content was analyzed by inductively coupled plasma-optical emission spectroscopy. Sulfate and nitrate anions formation was monitored by an ion chromatography system (ICS-2500, Thermo Fisher Scientific Inc., United States). The concentration of H_2O_2 was measured through a titanium (IV) oxysulfate method via UV–Vis spectrophotometer at wavelength of 400 nm (Kuang et al., 2011). The acute toxicity was tested with the luminescent bacterium Q67 (Vibrio qinghaiensis) was tested with bioluminescent bacterium (Tian et al., 2014). The electron spin resonance (ESR) spectra of typical ROS involved in this system were monitored with EPR spectrometer (JES-FA200, Bruker, Germany). The ROS will react with corresponding spin-trapping reagents 5,5-dimethyl-1-pyrroline N-oxide (DMPO) or tetramethylpiperidinooxy (TMP) to form spin adducts either in water or methanol. To identify the chemical structures of trace amount of MB degradation intermediates adsorbed on the solid surface of β-FeOOH@GO after degradation, a TOF-SIMS V system (IONTOF GmbH Inc., Germany) was applied. To analyze the degradation intermediates of MB present in the solution, a Waters Acquity UPLC/MS (Waters Ltd., USA) was used and equipped with a BEH C18 analytical column (1.7 μm, 2.1 × 50 mm).

3. Results and discussion

β-FeOOH@GO was synthesized through a simplest and moderate way by in-situ hydrolysis of $FeCl_3$ in presence of GO (Iiu et al., 2016). Monodispersed rice-spike like β-FeOOH nanorods uniformly distributed on the wrinkled transparent surface of layered GO nanosheet with the uniform dimensions of about 100 nm of length × about 20 nm of width shown in Fig. S1. The intercalated β-FeOOH nanorods within the lamellar organization of GO prevents the restacking of GO nanosheetes and decreases the integrity of graphene oxide crystal structure, leading to the disappearing of the diffraction peaks corresponding to GO. The iron content of β-FeOOH@GO was determined to be 25.8%, higher than the iron content of iron oxide impregnated resins (7–12%), activated carbon (7%) and sand (1–3%) (DeMarco et al., 2003; Katsoyiannis and Zouboulis, 2002; Vaughan and Reed, 2005). The surface area and porosity are 202.6 $m^2 g^{-1}$ and with mesopore volume distribution of 74% and micro or macropore volume distribution of 13%,

separately (Kuang et al., 2016). Due to the unique properties of GO, the potential catalytic ability of β-FeOOH@GO was evaluated through decolorization of MB in photo-Fenton-like system.

3.1. Enhanced decolorization performance of β-FeOOH@GO in photo-Fenton-like system

The decolorization efficiencies of MB by adsorption, UV irradiation, Fenton-like and photo-Fenton-like processes were studied and results were shown in Fig. 1A. The decolorization ratio of MB by β-FeOOH and β-FeOOH@GO was 7.7% and 62.4 after 60 min mainly due to the adsorption, respectively. β-FeOOH@GO showed a significant enhanced adsorption capacity in contrast to that of β-FeOOH due to the superior adsorption and enrichment ability of GO which would strongly interact with MB through electrostatic and π-π stacking interactions (Kim et al., 2015; Zhao et al., 2012). Decolorization ratio of MB with UV photolysis, β-FeOOH + UV and β-FeOOH@GO + UV was 20.3%, 7.7% and 79.3% after 60 min reaction, respectively. The MB decolorization of by β-FeOOH@GO + UV photocatalysis was greatly improved comparing with β-FeOOH + UV mainly ascribed to the strong adsorption ability of GO. β-FeOOH and β-FeOOH@GO did not yield decolorization in the presence of H_2O_2 in relation to their relevant adsorption results, indicating that the Fenton-like processes of β-FeOOH and β-FeOOH@GO contributed pretty weak in MB decolorization. Decolorization of MB by H_2O_2+UV, photo-Fenton-like systems of β-FeOOH + H_2O_2+UV and β-FeOOH@GO + H_2O_2+UV was 94.4%, 96.1% and 99.7% after 60 min, respectively. The pseudo-first order rate constants of MB decolorization in control experiments were shown in Table S1. The pseudo-first order rate constants of MB decolorization in β-FeOOH + H_2O_2+UV and β-FeOOH@GO + H_2O_2+UV systems were 0.2148 min^{-1} and 0.6322 min^{-1}, respectively. The synergistic interaction of GO and β-FeOOH not only mediates the physiochemical and optical property of β-FeOOH but also effectively concentrates large amount of MB in the vicinity of β-FeOOH leading to greatly enhanced catalytic activity of β-FeOOH@GO.

The optical absorption properties of β-FeOOH@GO were investigated through UV–Vis diffuse reflectance spectra (UV–Vis DRS) and photoluminescence spectra (PL). In Fig. 1B, the pristine β-FeOOH has an absorption edge at approximately 630 nm ascribed to the band gap of ~1.88 eV β-FeOOH@GO exhibits stronger light absorption ability and a significant photosensitivity in both visible and UV regions due to interfacial interaction between β-FeOOH with GO sheets. In Fig. 1C, the PL spectrum of β-FeOOH showed that numerous photo-induced charges were easily generated under irradiation. β-FeOOH@GO showed obvious PL quenching effect revealing the strong electronic interaction between β-FeOOH and GO sheets. The photogenic electrons can be effectively transferred from GO surface to β-FeOOH under UV irradiation leading to promote the photo-reduction of Fe^{3+} to Fe^{2+} on the surface of β-FeOOH@GO heterojunction due to GO's large electron storage capacity (Cai et al., 2015; Tian et al., 2013), greatly enhanced photo-Fenton-like catalytic performance (Yao et al., 2014).

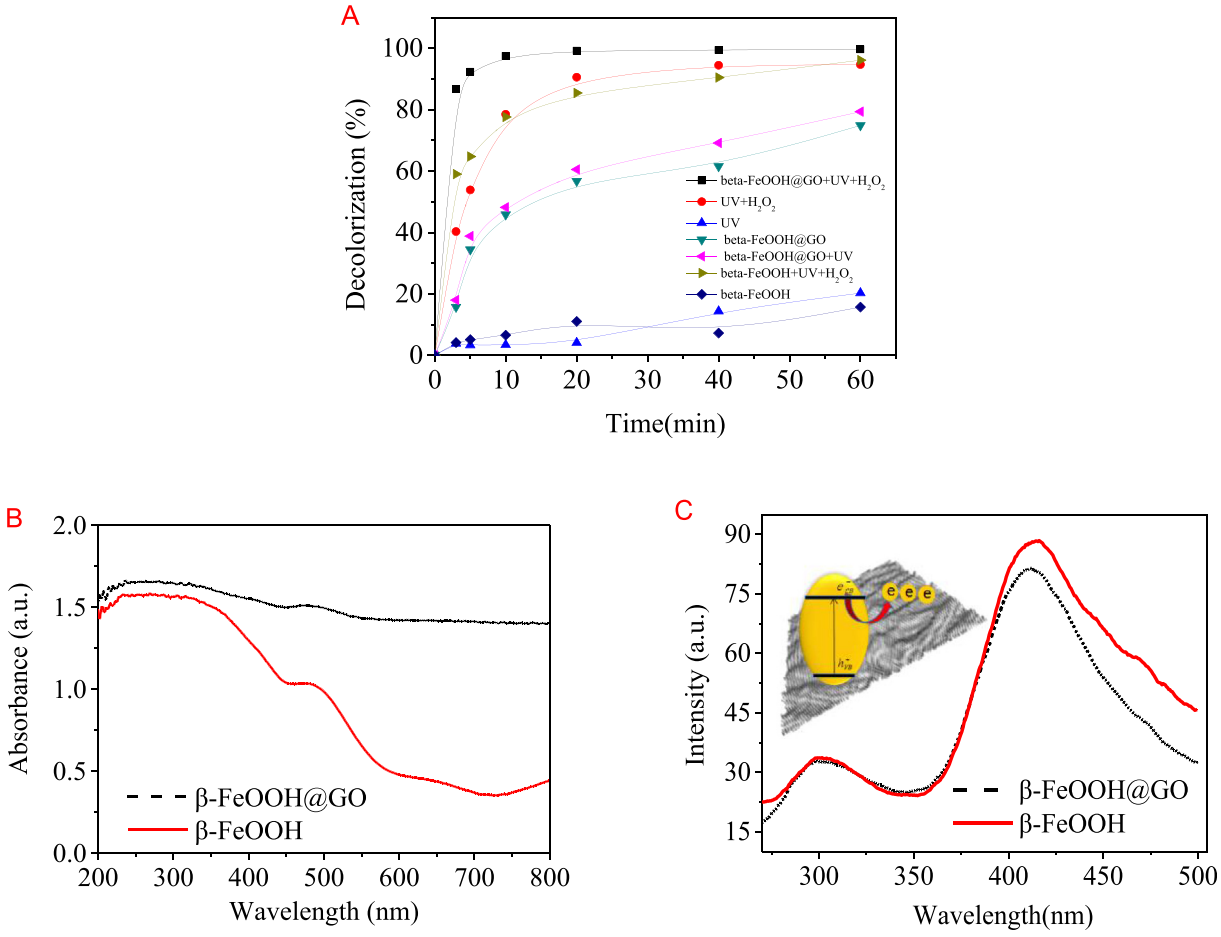

Fig. 1. Decolorization of MB under different conditions (A), UV–Vis DRS (B) and PL spectra (C) of β-FeOOH and β-FeOOH@GO.

3.2. Effect of pH

The effect of pH on decolorization of MB in β-FeOOH@GO + H_2O_2+UV system was shown in Fig. 2A. The β-FeOOH@GO + H_2O_2+UV system maintained efficiently in decolorizing MB within pH ranges from 2.67 to 12.11. The point of zero charge (pH_{ZPC}) of β-FeOOH@GO was determined to be 2.25 due to the presence of GO (Kuang et al., 2016). The surface of β-FeOOH@GO would be negatively charged at higher pH value (pH > 2.25), thus facilitating favorable adsorption of the cationic dye of MB through electrostatic attraction. The temporal consumption of H_2O_2 with time in three different pH values was also detected and shown in Fig. 2B. H_2O_2 consumption decreased or more likely to be activated in the sequence of alkaline (pH = 12.11) > neutral (pH = 5.60) > acid (pH = 2.67) in this system, separately (Yuan et al., 2013). Another reason would be lower pH values protonating H_2O_2 and disfavoring the formation of ·OH radicals (De Laat and Gallard, 1999). It suggested that β-FeOOH@GO catalyzed heterogeneous Fenton-like process has greatly expanded the efficient application pH range. Wang et al. reported the decolorization of MB was nearly 100% in photo-Fenton-like process catalyzed by Fe(II)Fe(III)-LDHs in pH of 2–7, while decolorization decreased to 76.4% when the pH increased to 10 (Wang et al., 2014). He et al. also reported dye of MY10 was nearly decomposed in α-FeOOH + H_2O_2+UV system within 120 min at pH 5, and it needed about 340 min to complete removal at pH 9 (He et al., 2002; Poulios et al., 2003). Shao et al. reported the RhB decolorization rate decreased from 92% to 64% in α-Fe_2O_3-graphene H_2O_2+visible light when pH increased from 3 to 9 (Shao et al., 2015). Comparing with those reports, in whole pH range β-FeOOH@GO could improve the interaction between MB with β-FeOOH in microenvironment.

3.3. Effect of H_2O_2 dose

The effect of H_2O_2 dosage on MB decolorization in β-FeOOH@GO + H_2O_2+UV system was shown in Fig. 3. The decolorization of MB increased with the addition of more amount of H_2O_2 in this system. Commonly, Fenton reaction uses dozens of to thousands of equivalents of H_2O_2 with respect to the pollutants (Dhakshinamoorthy et al., 2012; Navalon et al., 2010). For example, the molar ratio of H_2O_2 to dyes in photo-Fenton-like reaction was 74 in decolorization of red B catalyzed by Fe_2O_3 supported on activated carbon fibers (Lan et al., 2015), was 83 in Rhodamine B decolorization catalyzed by α-Fe_2O_3-graphene (Shao et al., 2015), was 2807 in MB decolorization catalyzed by Fe_3O_4@rGO@TiO_2 (Yang et al., 2015), was 3500 in Orange II decolorization catalyzed by $ZnFe_2O_4$-g-C_3N_4 (Yao et al., 2014), was 4163 in Rhodamine B decolorization catalyzed by GO–$FePO_4$ (Guo et al., 2015) and was

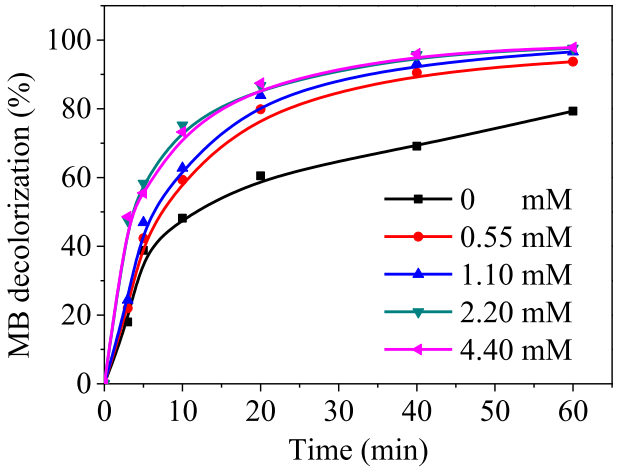

Fig. 3. Effect of H_2O_2 dosage on MB decolorization in β-FeOOH@GO + H_2O_2+UV system.

5069 in methyl orange decolorization catalyzed by Fe_2O_3-graphene aerogels (Qiu et al., 2015), respectively. The complete mineralization of MB using minimum dosage of H_2O_2 is highly desired for practical application. In this study, nearly a hundred percent of MB removal is obtained in β-FeOOH@GO + H_2O_2+UV system with the molar ratio of H_2O_2 to MB of 10. Addition of more H_2O_2 could enhance the generation of ·OH and photocatalytic efficiency (Ma et al., 2015), while, the addition of excess amount of H_2O_2 would not be helpful in promoting MB decolorization because of H_2O_2 acting as the ·OH radicals quencher (Hadjltaief et al., 2013; Kuang et al., 2013).

3.4. Durability of β-FeOOH@GO

In order to further testify whether β-FeOOH@GO was regenerated in-situ, six times consecutive degradation recycles of regeneration in β-FeOOH@GO + H_2O_2+UV system were conducted and the result was presented in Fig. 4A. The adsorption of MB of β-FeOOH@GO was slight lower than that of the first time after the 6th reuse due to occupation of adsorption sites by the degradation intermediates of MB or partly the loss of a small amount of the catalyst in the recycling runs; while the MB degradation patterns and efficiency remained similar with that of the first cycle. The FTIR of β-FeOOH@GO after 6 time photo-Fenton-like oxidation shown in Fig. 4B was basically identical with that of the original β-FeOOH@GO (Iiu et al., 2016). The MB mineralization and generation of anions at natural pH in the first cycle in this system were also

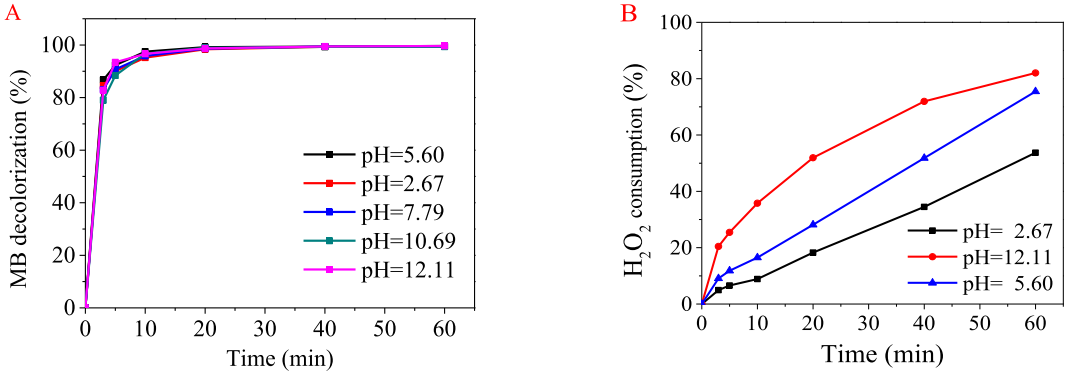

Fig. 2. Effect of pH on MB decolorization (A) and H_2O_2 decomposition (B) in β-FeOOH@GO + H_2O_2+UV system.

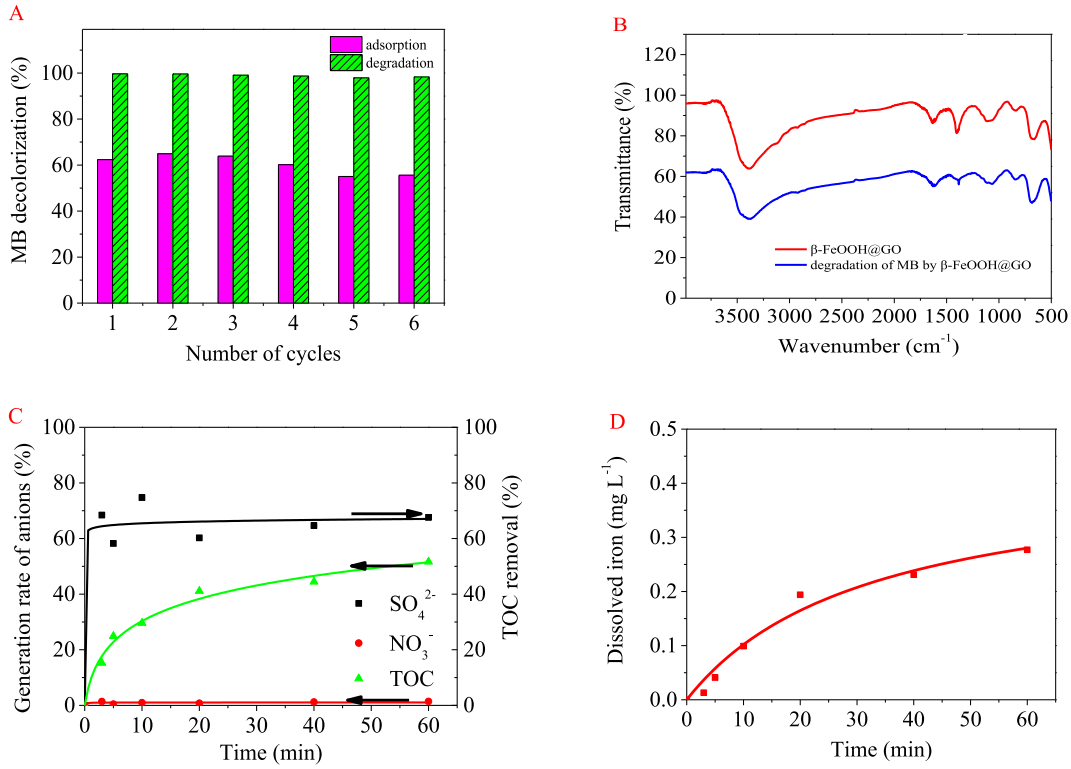

Fig. 4. Durability of the catalyst after 6 times recycles (A) and FTIR spectra of β-FeOOH@GO before or after degradation of MB (B); generation of SO_4^{2-}, NO_3^-, mineralization (C) and dissolved iron content (D) in β-FeOOH@GO + H_2O_2+UV systems.

presented in Fig. 4C. It can be deduced that C–S^+=C group in thionin ring was firstly attacked by ·OH radicals according to the occurrence of predominant SO_4^{2-} anions sharply reaching 70% at initial 3 min reaction. By contrast, the generation of NO_3^- nearly kept a constant level at about 1% throughout the reaction, showing insignificant N-demethylation intermediates occurred during the process (Houas et al., 2001). The organic carbon (TOC) removal continued to rise with the reaction time until up to 50% at 60 min. In Fig. 4D, the maximum dissolved iron was 0.277 mg L^{-1} which accounts for 0.4% of doped β-FeOOH. The photo-dissolution of β-FeOOH@GO was not significant in the reactions due to the strong chemical interaction between β-FeOOH with GO (Lachheb et al., 2002). Therefore, the homogeneous photo Fenton pathway hardly made contribution to MB decolorization induced by lower concentration of dissolving iron species. Iron species are therefore recycled directly on the catalyst without significant diffusion into the solution.

3.5. Photo Fenton-like catalytic degradation mechanism

3.5.1. Evolution profile of UV–Vis absorbance of MB decolorization

Temporal changes of the UV–Vis spectra during MB degradation was given in Fig. 5. The maximum absorption peaks in the visible range at 665 and 610 nm were attributed to the chromophores of MB namely –C=S and –C=N and its dimers, which can undergo hemolytic cleavage (Zhou et al., 2010a). The peaks at 245 and 292 nm was ascribed to the $\pi \rightarrow \pi^*$ transition related to conjugated aromatic rings (Li and Zhang, 2010). Fig. 5 showed a dramatic decrease of MB absorbance with the reaction proceeding implies the breakdown of conjugated system of phenothiazine chromophores accompanying the degradation of auxochrome of benzene ring in MB structure. It indicated that the decolorization of MB and decomposition of benzene ring occurred at the same time (Yu et al., 2015). In addition, absorbance at a lower UV region around 200 nm increased firstly then gradually decreased due to the first formation of benzene cleavage intermediates finally leading to the mineralization (Zaied et al., 2011). It should be noted that the absorbance around 200 nm does not completely disappear after 60 min, owing to the accumulation of unsaturated hydrocarbon intermediates. An insignificant hypochromic-shift occurred from 665 nm (λ_{max} for MB) to 630 nm with intensity descending within 10 min which was shown in inset of Fig. 5, which suggests a minor N-demethylation of MB occurred. Wen-Hui Kuan et al. reported a marked blue-shift of

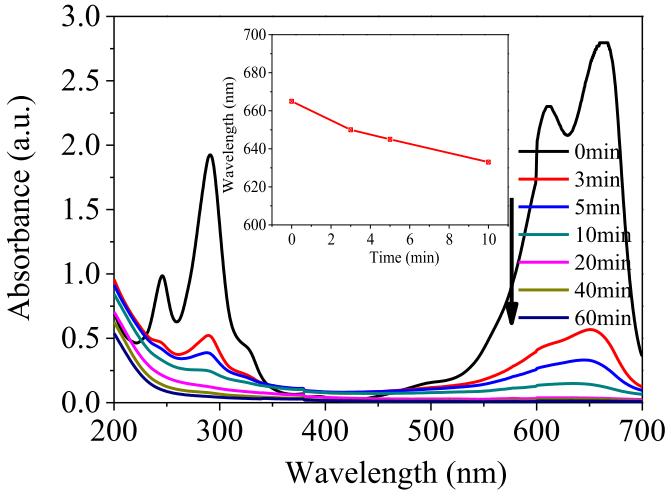

Fig. 5. The temporal evolution of UV–Vis spectra of MB decolorization in β-FeOOH@GO + H_2O_2+UV system (inset: shift of maximum absorption wavelength as a function of reaction time).

UV–Vis absorbance peaks of MB in the MnO_2 or MnO_2/heating systems. In sole MnO_2 system, the UV–Vis absorbance peak of MB shifted from 665 nm (λ_{max} for MB) to 650 nm (λ_{max} for Azure B) at a reaction time of 5 min and then shifted to 600 nm (λ_{max} for Thionin) after 24 h. In MnO_2/heating system, two distinguished peaks at 640 nm (λ_{max} for Azure A) to 618 nm (λ_{max} for Azure C) were observed at 5 min, in which N-demethylation of MB containing auxochromic methylamine groups is another important catalytic degradation pathway (Kuan et al., 2013). Wu et al. also observed the obviously blue-shift at 665 nm resulting from the formation of demethylated dyes intermediates (Wu et al., 2015). In our study, the blue-shift gradually became clear due to formation of N-demethylation by-products of MB within 10 min. It suggested N-demethylation was probable part of the reaction pathway of MB decolorization in β-FeOOH@GO + H_2O_2+UV system.

3.5.2. Proposed degradation pathway of MB

In order to verify MB degradation was a surface-catalyzed reaction on the interface of β-FeOOH@GO/water, the surface analysis of β-FeOOH@GO was first time reported through TOF-SIMS in our study and the result was shown in Fig. S2. TOF-SIMS can precisely identify the trace amount of organics on the surface of a solid material. Many fragments with different m/z were coappeared in negatively and positively charged mass spectra, such as $m/z = 302$, 312, 317, 284 (molecular weight of MB), 255, 201, 325, 341, 357. The formation of those MB degradation intermediates adsorbed on the surface of β-FeOOH@GO identified with TOF-SIMS confirmed the surface-catalytic nature of this heterogeneous Fenton-like system.

The degradation intermediates of MB present in aqueous solution was further analyzed by LC-ESI(+)-MS shown in Fig. S3 reconfirming the TOF-SIMS' results. The peaks with different m/z, such as 263, 279, 301, 317 and 342 were observed both in TOF-SIMS and LC-MS analysis which clearly indicated that the surface adsorbed MB degradation intermediates will ultimately diffuse into the bulk solution. Based on the nitrate or sulfate anions formation, TOF-SIMS and LC-MS spectra, the predominant degradation pathway was proposed firstly to oxide C–S^+=C groups of thionine ring to form the intermediates from $m/z = 284$ to 301, 317, 255 rather than to oxide dimethylamino groups. The peak with $m/z = 255$ indicates the rupture of thionine ring through desulphone reaction to release high concentration of sulfate anions, which induces the opening of central heterocylic ring of phenothiazine structure. The peaks with $m/z = 263$, 279, 295 and 312 indicated the subtraction of sulfur dioxides from the relative parent compounds accordingly. The demethylation reaction proved by the blue-shifts of the maximum absorption peak of MB also occurred simultaneously accompanying with the main desulfonation reaction with the formation of intermediates with $m/z = 270$, 256, 241 and 198. Besides, other minor reaction pathways of dedimethylation or dedimethylamino reaction were also identified. For example, two symmetrical dimethylaminos groups on thionine ring of $m/z = 317$ can be successively hydroxylated by replacement of dimethylamino groups to produce $m/z = 325$, 341 and 357. The oxidation of imino-group groups in central rings would be obtained by hydroxyl radicals to form aniline and finally oxided to nitrate anions. Those three degradation pathways were consistent with the bond dissociation energy theory in the sequence of C–S^+=C (76 kcal mol^{-1}) < C–N=C (87.4 kcal mol^{-1}) < $N(CH_3)_2$–C_6H_5 (93.2 kcal mol^{-1}) < H_2N–C_6H_5 (10.2.6 kcal mol^{-1}) (Huang et al., 2010). The lower the bond dissociation energy was, the easier the bond was broken. In our study C–S^+=C was first to be attacked by ROS rather than C–N mainly due to the strong interaction between positive MB with negative GO carriers of β-FeOOH@GO.

A possible detailed degradation pathway for MB degradation in β-FeOOH@GO + H_2O_2+UV system was proposed in Scheme 1. The desulfuration pathway of MB degradation, all newly identified sulfoxide or sulphone intermediates formed by oxidation of C–S^+=C groups, desulfuration intermediates excepting $m/z = 270$, 256, 242 and 199, and demethylation or dedimethylamino intermediates of MB were firstly reported in our study. The desulfonation reaction was the predominant degradation pathway in our β-FeOOH@GO + H_2O_2+UV treatment, which was obviously different with previous reports (Kuan et al., 2013; Wu et al., 2015; Zhang et al., 2002). Kuan et al. mainly reported the formation of N-demethylation intermediates such as Azure A ($m/z = 256$), Azure B ($m/z = 270$), Azure C ($m/z = 242$) and phenothiazine ($m/z = 199$) and inorganic nitrate anions as the important catalytic degradation pathway when MB was decomposed in the MnO_2 or MnO_2/heating systems (Kuan et al., 2013). Similar studies were also reported elsewhere (Wu et al., 2015; Zhang et al., 2002). Huang et al. reported five degradation intermediates of MB with $m/z = 135$, 108, 91, 82 and 69 analyzed by GC-MS, which were formed by rupturing of thionine ring using the dielectric barrier discharge technique (Huang et al., 2010). Batista et al. reported the demethylation intermediates analyzed with LC-MS with $m/z = 270$ (reducing one $-CH_3$) and hydroxylation intermediates on benzene rings with $m/z = 300$ (adding one hydroxyl), 316 (adding two hydroxyls) and 332 (adding three hydroxyls) of MB degradation photocatalyzed by CuO/SiO_2 (Batista et al., 2008). One sulfoxide intermediate with the rupturing of thionine ring with $m/z = 303$ was identified with LC-MS when MB was photocatalyzed by TiO_2 in water (Houas et al., 2001). The by-products of MB detected using LC-MS and reaction pathway proposed in previous work in literature are greatly extended through TOF-SIMS surface analysis.

The oxidation of organic contaminants would change the toxicity to living things (Andreozzi et al., 2006; Buser et al., 1999; Chaabane et al., 2007). In this study, luminous bacteria (Vibrio qinghaiensis), was used to evaluate the toxicity of MB and its degradation intermediates, the results were described in Fig. S4. The relatively luminosity intensity of MB was about 6.8% and increased to 35.4% after 60 min reaction, which reflected an decreased toxicity of degradation intermediates with time. The declined toxicity may accompany the improvement of biodegradation of MB.

3.5.3. XPS analysis

The surface chemical states of iron, oxygen, nitrogen and carbon elements of β-FeOOH@GO before and after photodegradation of MB were conducted by XPS shown in Fig. 6. The photoelectron peaks located at binding energies of 712.1, 532.1, and 286.5 eV were assigned to the characteristic peaks of Fe 2p, O 1s, and C 1s of XPS wide survey spectrum (black line), respectively. The binding energy of N 1s is very sensitive to the chemical environment of nitrogen-containing groups. The binding energy of N 1s in heterocylic nitrogen is 398–400 eV, for example 398.6eV in pyridine and 399.5 in N–C bond. After degradation of MB, the peak of N 1s with binding energy of 398.2 eV of β-FeOOH@GO appeared (red line) which could be attributed to the presence of nitrogen functional groups. It implied that some imidogen-containing degradation intermediates of MB had been adsorbed on the surface of β-FeOOH@GO, which was consistent with TOF-SIMS results. The binding energy of N 1s was not shifting which implied MB adsorbed was exposing to the catalytic active center through positive sulfur groups rather than the $-NMe_2$ groups so that it won't lead to N-demethylation reaction to occur firstly or strongerly. The binding energy of S 2p (161.5–163.1eV) or S 2s (227.5–232.4eV) was not observed. The quick loss of sulfur from MB structure showed sulfur rather than the imidogen groups were firstly attacked by ROS (Houas et al.,

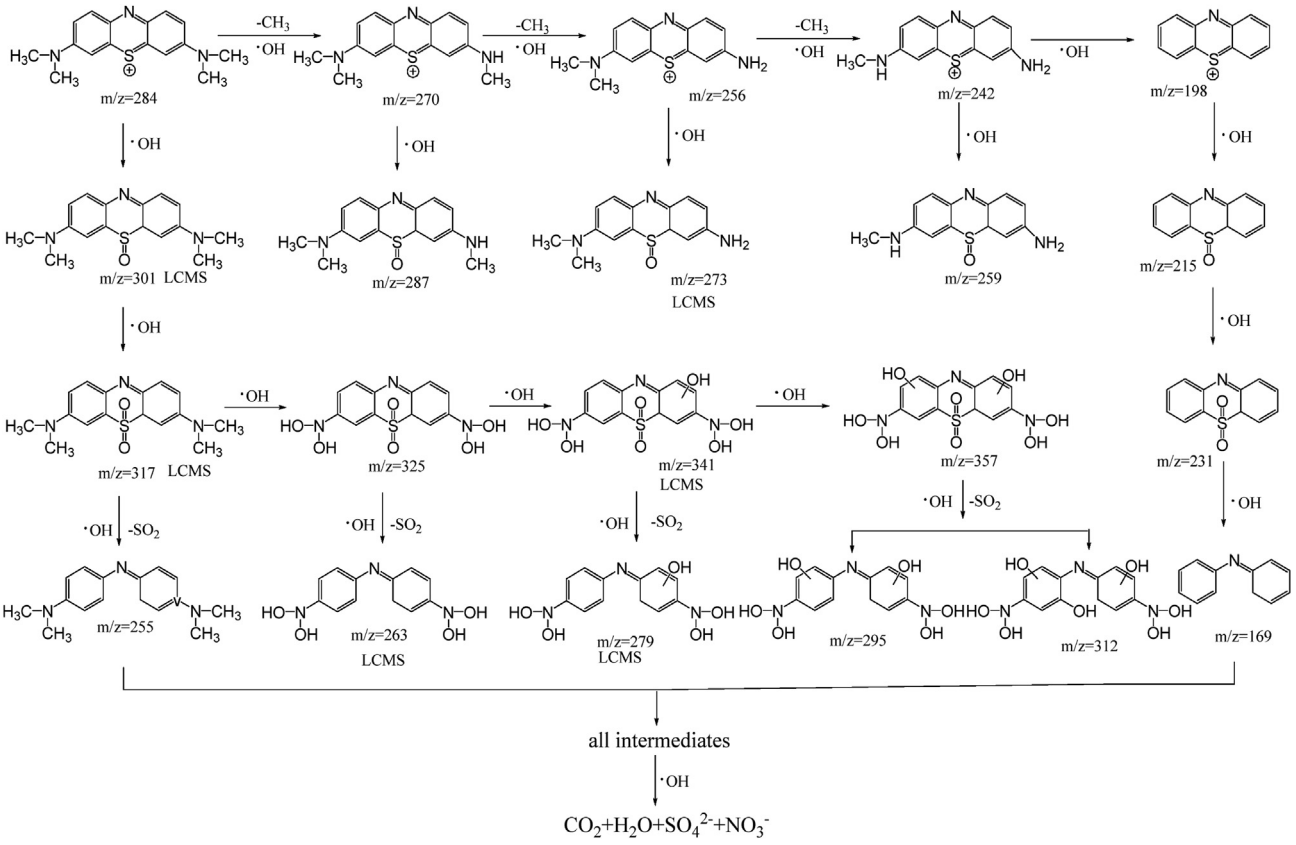

Scheme 1. Proposed degradation pathway of MB in β-FeOOH@GO + H_2O_2+UV system.

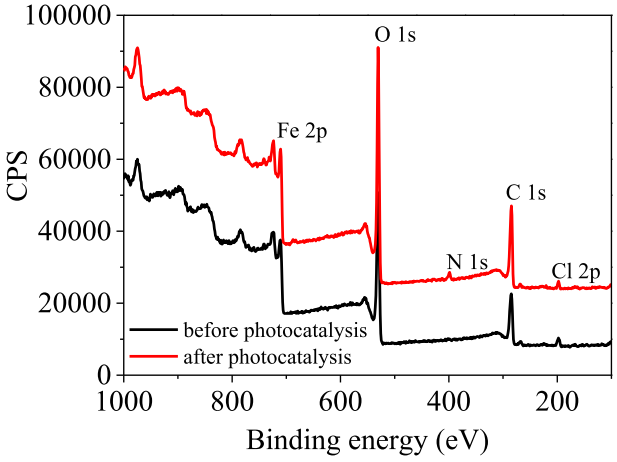

Fig. 6. XPS survey of catalyst before and after MB decolorization in β-FeOOH@GO + H_2O_2+UV system.

2001; Yu and Chuang, 2007).

The surface iron species of β-FeOOH@GO can be splitted into doublets of Fe $2p_{1/2}$: Fe $2p_{3/2}$. The intensity ratio of Fe^{2+}/Fe^{3+} was changed from 51:49 before degradation to 57:43 after degradation in Table 1. The efficient recycling of between surface Fe^{2+} and Fe^{3+} species or efficient reduction from surface Fe^{3+} to Fe^{2+} of β-FeOOH@GO effectively ensure the pretty well catalytic activity of β-FeOOH@GO + H_2O_2+UV system. For the O 1s line can be deconvoluted into five peaks which were corresponding to lattice oxygen atoms binding with Fe (Fe—$O_{lattice}$), lattice hydroxyl (Fe—$OH_{lattice}$), surface adsorbed hydroxyl (Fe—OH_{ad}), surface adsorbed water (Fe—H_2O_{ad}), and Fe—O—C interaction bonds, respectively (Zhou et al., 2010b). The new occurrence of Fe—O—C bond in β-FeOOH@GO further proves the formation of heterojunction between β-FeOOH and GO. The heterojunction of β-FeOOH@GO will greatly mediate the physiochemical property and photocatalytic performance. The decreasing intensity of surface adsorbed hydroxyl signal in catalytic active center after degradation suggested that the hydroxyl groups took an active part in the degradation of MB.

3.5.4. Catalytic mechanism

Fenton-like catalytic reaction might be mainly originated from Fe^{2+}-mediated on the boundary of β-FeOOH nanoparticles rather than Fe^{3+}-mediated. ·OH and $O_2^{\bullet-}$ were proved as important ROS in Fenton-like systems (Bissey et al., 2006; Ruales-Lonfat et al., 2015; Smith et al., 2004). In this study, ERS trap technique was used to identify the main ROS involved in β-FeOOH@GO + H_2O_2+UV system and the results were shown in Fig. 7. The characteristic peaks of DMPO-OH, DMPO-OOH and TEMP-$^1O_2$ adducts were obviously observed with the intensity increasing with the irradiation time confirming the presence of ·OH, $HO_2^{\bullet}$ and singlet oxygen ($^1O_2$). ·OH radicals are well-known predominant radicals in Fenton reaction. The DMPO-OOH spectra was in good agreement with previous report confirming the formation of $HO_2^{\bullet}$ rather than $O_2^{\bullet}$(Bannister and Bannister, 1985). The DMPO can trap $HO_2^{\bullet}$ to form DMPO-OOH which is unstable directly breakdown to DMPO-OH adduct (Bannister and Bannister, 1985). Usually, $O_2^{\bullet-}$ radicals can be formed through one-electron transfer reduction of oxygen on the surface of catalyst. While the ERS spectra of DMPO-$O_2^{\bullet-}$ adducts was not observed either due to its short relaxation half-life or nonexistence

Table 1
Binding energy and atomic surface concentration of detected elements of β-FeOOH@GO.

	Binding energy (eV)								
	Fe								
	2p3/2	2p1/2			O 1s			C 1s	N 1s
Before	710.9	726.3	529.8	531.1	532.4	533.3	534.2	284.6	0
After	710.6	726.3	529.7	531.1	532.3	533.2	534.1	284.6	398.2
Atomic mass surface concentration (%)									
	Fe		O					C	N
	Fe^{2+}	Fe^{3+}			Fe-OH_{ads}	H_2O_{ads}	−C−O−Fe		
Before	25.77				38.52			35.70	0
	50.7%	49.3%	13.8%	24.4%	28.2%	19.9%	13.7%		
After	22.11				37.43			38.96	1.50
	57.3%	42.7%	15.6%	30.5%	26.3%	17.8%	9.8%		

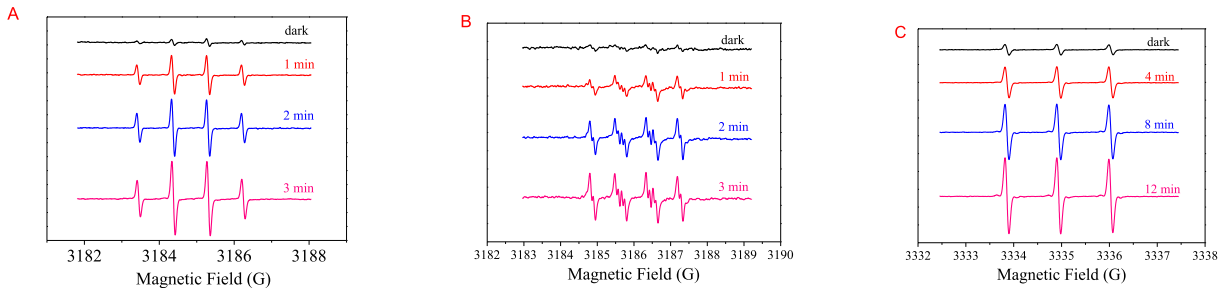

Fig. 7. ESR spectra of the DMPO-OH (A), DMPO-OOH (B) and TEMP-$^1O_2$ (C) adducts recorded in β-FeOOH@GO + H_2O_2+UV system.

(Bannister and Bannister, 1985). It is interesting to find the presence of $^1O_2$ which was seldom reported in previous works (Bissey et al., 2006; Ruales-Lonfat et al., 2015; Smith et al., 2004).

Accordingly, a possible main mechanism for degradation of MB in β-FeOOH@GO + H_2O_2+UV system was proposed: 1) the MB molecule was adsorbed onto the catalyst through electrostatic interaction and π-π stacking; 2) ˙OH radicals produced by H_2O_2 activated with photoreduced Fe^{2+} on the surface of β-FeOOH@GO; and 3) Adsorbed MB was attacked by ˙OH. The increased number of accessible active sites and effective enrichment of MB around catalytic center of β-FeOOH@GO was guaranteed by the introduction of GO (Vinothkannan et al., 2015). The GO has strong interaction

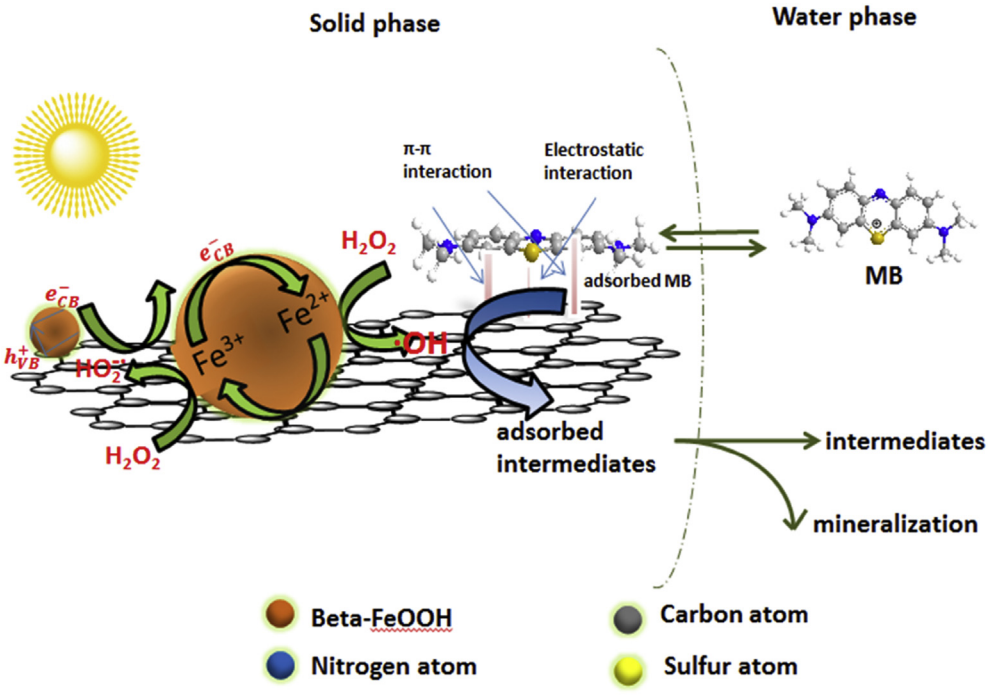

Scheme 2. Possible catalytic oxidation mechanism of MB in β-FeOOH@GO + H_2O_2+UV system.

with β-FeOOH due to formation C–O–Fe chemical bond in β-FeOOH@GO which would cause charge redistribution at GO/β-FeOOH interface. As super electronic acceptor and donor, GO can easily capture the photogenic electrons (e_{CB}^-) from the conducting band of semiconductors or LUMO energy of dyes. The captured e_{CB}^- can quickly transfer from GO to the activated catalytic sites of β-FeOOH due to this heterojunction of β-FeOOH@GO. The Fe^{3+} on the surface of β-FeOOH@GO can be efficiently reduced to Fe^{2+} by reacting with $h\nu$, H_2O_2 or e_{CB}^- on the surface of GO, which would synergistically enhance the photo Fenton-like catalytic performance of β-FeOOH@GO (Meng et al., 2013). The introduction of GO greatly enhances transformation from Fe^{3+} to Fe^{2+} or recycling of iron specie. The recycle of iron oxidation states or the bottleneck of Fenton reaction could be speed up through this photo-assisted Fenton-like reaction as following:

(GO≡β − FeOOH represents the β − FeOOH@GO)

$$GO{\equiv}\beta - FeOOH + hV \rightarrow GO{\equiv}\beta - FeOOH\left(e_{CB}^- + h_{VB}^+\right) \quad (1)$$

The e_{CB}^- can be transferred from GO to GO≡β-FeOOH–Fe^{3+}

$$GO{\equiv}\beta - FeOOH - Fe^{3+} + e_{CB}^- \rightarrow GO{\equiv}\beta - FeOOH - Fe^{2+} \quad (2)$$

$$GO{\equiv}\beta\text{-}FeOOH\text{-}Fe^{3+} + H_2O_2 \rightarrow GO{\equiv}\beta\text{-}FeOOH\text{-}Fe^{2+} + HO\bullet_2^- + H^+ \quad (3)$$

$$GO{\equiv}\beta\text{-}FeOOH\text{-}Fe^{3+} + HO_2^{\bullet -} \rightarrow GO{\equiv}\beta\text{-}FeOOH\text{-}Fe^{2+} + O_2 + H^+ \quad (4)$$

$$GO{\equiv}\beta\text{-}FeOOH\text{-}Fe^{2+} + H_2O_2 \rightarrow GO{\equiv}\beta\text{-}FeOOH\text{-}Fe^{3+} + \bullet OH + OH^- \quad (5)$$

$$HO_2^{\bullet -} + HO_2^{\bullet -} \rightarrow H_2O_2 + H_2O \quad (6)$$

$$\bullet OH/HO_2^{\bullet -} + \text{dye} \rightarrow \text{intermediates} \rightarrow \text{mineralization} \quad (7)$$

The possible photocatalytic mechanism of β-FeOOH@GO in decolorizing MB was depicted in Scheme 2.

4. Conclusions

Fe^{2+} and Fe^{3+} a very common environmental redox couples. Their redox reaction was linked with the formation of adsorbed Fe^{2+} species on the surface of catalyst. The β-FeOOH@GO + H_2O_2+UV Fenton-like system would be a highly efficient, artificially intensified physiochemical technology in treating high concentration organic pollutants at broad pH range of application. The MB degradation intermediates were fully identified through combining with TOF-SIMS and LC-MS, which was very important for sewage treatment process upgrading. The toxicity of the photocatalytic degradation intermediates of the MB samples was much lower than that of parent compound, illustrating the technology without producing more toxic intermediates of MB. Hence, β-FeOOH@GO could be a promising bifunctional composite either as adsorbent or as heterogeneous Fenton-like catalyst in eliminating the environmental refractory pollutants and its relative toxicity.

Acknowledgements

We are appreciated for the support from the National Natural Science Foundation of China (No. 21377039).

Appendix A. Supplementary data

Supplementary data to this article can be found online at https://doi.org/10.1016/j.chemosphere.2018.11.098.

References

Andreozzi, R., Canterino, M., Lo Giudice, R., Marotta, R., Pinto, G., Pollio, A., 2006. Lincomycin solar photodegradation, algal toxicity and removal from wastewaters by means of ozonation. Water Res. 40, 630–638.
Bae, S., Kim, D., Lee, W., 2013. Degradation of diclofenac by pyrite catalyzed Fenton oxidation. Appl. Catal. B Environ. 134, 93–102.
Banat, I.M., Nigam, P., Singh, D., Marchant, R., 1996. Microbial decolorization of textile-dye-containing effluents: a review. Bioresour. Technol. 58, 217–227.
Bannister, J.V., Bannister, W.H., 1985. Production of oxygen-centered radicals by neutrophils and macrophages as studied by electron spin resonance (ESR). Environ. Health Perspect. 64, 37–43.
Barrios-Ziolo, L.F., Gaviria-Restrepo, L.F., Agudelo, E.A., Cardona-Gallo, S.A., 2015. Technologies for the removal of dyes and pigments present in wastewater. A Review 82, 118–126.
Batista, A.P.L., Carvalho, H.W.P., Luz, G.H.P., Martins, P.F.Q., Gonçalves, M., Oliveira, L.C.A., 2008. Preparation of CuO/SiO_2 and photocatalytic activity by degradation of methylene blue. Environ. Chem. Lett. 8, 63–67.
Bissey, L.L., Smith, J.L., Watts, R.J., 2006. Soil organic matter-hydrogen peroxide dynamics in the treatment of contaminated soils and groundwater using catalyzed H_2O_2 propagations (modified Fenton's reagent). Water Res. 40, 2477–2484.
Bossmann, S.H., Oliveros, E., Gob, S., Siegwart, S., Dahlen, E.P., Payawan, L., Straub, M., Worner, M., Braun, A.M., 1998. New evidence against hydroxyl radicals as reactive intermediates in the thermal and photochemically enhanced fenton reactions. J. Phys. Chem. 102, 5542–5550.
Brillas, E., Martinez-Huitle, C.A., 2015. Decontamination of wastewaters containing synthetic organic dyes by electrochemical methods. An updated review. Appl. Catal. B Environ. 166, 603–643.
Buser, H.R., Poiger, T., Muller, M.D., 1999. Occurrence and environmental behavior of the chiral pharmaceutical drug ibuprofen in surface waters and in wastewater. Environ. Sci. Technol. 33, 2529–2535.
Cai, L., Xiong, X.L., Liang, N.G., Long, Q.Y., 2015. Highly effective and stable Ag_3PO_4-WO_3/MWCNTs photocatalysts for simultaneous Cr(VI) reduction and orange II degradation under visible light irradiation. Appl. Surf. Sci. 353, 939–948.
Chaabane, H., Vulliet, E., Joux, F., Lantoine, F., Conan, P., Cooper, J.F., Coste, C.M., 2007. Photodegradation of sulcotrione in various aquatic environments and toxicity of its photoproducts for some marine micro-organisms. Water Res. 41, 1781–1789.
Chowdhury, S., Balasubramanian, R., 2014. Graphene/semiconductor nanocomposites (GSNs) for heterogeneous photocatalytic decolorization of wastewaters contaminated with synthetic dyes: a review. Appl. Catal. B Environ. 160, 307–324.
De Laat, J., Gallard, H., 1999. Catalytic decomposition of hydrogen peroxide by Fe(III) in homogeneous aqueous solution: mechanism and kinetic modeling. Environ. Sci. Technol. 33, 2726–2732.
DeMarco, M.J., Sengupta, A.K., Greenleaf, J.E., 2003. Arsenic removal using a polymeric/inorganic hybrid sorbent. Water Res. 37, 164–176.
Dhakshinamoorthy, A., Navalon, S., Alvaro, M., Garcia, H., 2012. Metal nanoparticles as heterogeneous fenton catalysts. Chemsuschem 5, 46–64.
Espinosa, J.C., Navalon, S., Primo, A., Moral, M., Sanz, J.F., Alvaro, M., Garcia, H., 2015. Graphenes as efficient metal-free fenton catalysts. Chem. A European J. 21, 11966–11971.
Guo, S., Zhang, G., Yu, J.C., 2015. Enhanced photo-Fenton degradation of rhodamine B using graphene oxide-amorphous $FePO_4$ as effective and stable heterogeneous catalyst. J. Colloid Interface Sci. 448, 460–466.
Hadjltaief, H.B., Da Costa, P., Galvez, M.E., Ben Zina, M., 2013. Influence of operational parameters in the heterogeneous photo-fenton discoloration of wastewaters in the presence of an iron-pillared clay. Ind. Eng. Chem. Res. 52, 16656–16665.
He, J., Ma, W.H., He, J.J., Zhao, J.C., Yu, J.C., 2002. Photooxidation of azo dye in aqueous dispersions of H_2O_2/alpha-FeOOH. Appl. Catal. B Environ. 39, 211–220.
He, Z.M., Guai, G.H., Liu, J., Guo, C.X., Loo, J.S.C., Li, C.M., Tan, T.T.Y., 2011. Nanostructure control of graphene-composited TiO_2 by a one-step solvothermal approach for high performance dye-sensitized solar cells. Nanoscale 3, 4613–4616.
Houas, A., Lachheb, H., Ksibi, M., Elaloui, E., Guillard, C., Herrmann, J.M., 2001. Photocatalytic degradation pathway of methylene blue in water. Appl. Catal. B Environ. 31, 145–157.
Hu, X.B., Liu, B.Z., Deng, Y.H., Chen, H.Z., Luo, S., Sun, C., Yang, P., Yang, S.G., 2011. Adsorption and heterogeneous Fenton degradation of 17 alpha-methyltestosterone on nano Fe_3O_4/MWCNTs in aqueous solution. Appl. Catal. B Environ. 107, 274–283.
Huang, F., Chen, L., Wang, H., Yan, Z., 2010. Analysis of the degradation mechanism of methylene blue by atmospheric pressure dielectric barrier discharge plasma. Chem. Eng. J. 162, 250–256.
Iiu, Y., Lv, J., Jin, W., Zhao, Y., 2016. Defluoridation by rice spike-like akaganeite anchored graphene oxide. RSC Adv. 6, 11240–11249.
Jia, X.H., Song, H.J., Min, C.Y., 2013. Hydrothermal synthesis of flower-like TiO_2

nanocrystals/graphene oxide nanocomposites. Appl. Phys. Mater. Sci. Process 111, 1021–1024.
Katsoyiannis, I.A., Zouboulis, A.I., 2002. Removal of arsenic from contaminated water sources by sorption onto iron-oxide-coated polymeric materials. Water Res. 36, 5141–5155.
Kim, I.T., Magasinski, A., Jacob, K., Yushin, G., Tannenbaum, R., 2013. Synthesis and electrochemical performance of reduced graphene oxide/maghemite composite anode for lithium ion batteries. Carbon 52, 56–64.
Kim, H., Kang, S.O., Park, S., Park, H.S., 2015. Adsorption isotherms and kinetics of cationic and anionic dyes on three-dimensional reduced graphene oxide macrostructure. J. Ind. Eng. Chem. 21, 1191–1196.
Kuan, W.H., Chen, C.Y., Hu, C.Y., Tzou, Y.M., 2013. Kinetic modeling for microwave-enhanced degradation of methylene blue using manganese oxide. Int. J. Photoenergy 2013, 1–9.
Kuang, L.Y., Zhao, Y.P., Liu, L., 2011. Photodegradation of orange II by mesoporous TiO_2. J. Environ. Monit. 13, 2496–2501.
Kuang, Y., Wang, Q.P., Chen, Z.L., Megharaj, M., Naidu, R., 2013. Heterogeneous Fenton-like oxidation of monochlorobenzene using green synthesis of iron nanoparticles. J. Colloid Interface Sci. 410, 67–73.
Kuang, L., Liu, Y., Fu, D., Zhao, Y., 2016. FeOOH-graphene oxide nanocomposites for fluoride removal from water: acetate mediated nano FeOOH growth and adsorption mechanism. J. Colloid Interface Sci. 490, 259–269.
Lachheb, H., Puzenat, E., Houas, A., Ksibi, M., Elaloui, E., Guillard, C., Herrmann, J.M., 2002. Photocatalytic degradation of various types of dyes (Alizarin S, crocein orange G, methyl red, Congo red, methylene blue) in water by UV-irradiated titania. Appl. Catal. B Environ. 39, 75–90.
Lan, H.C., Wang, A.M., Liu, R.P., Liu, H.J., Qu, J.H., 2015. Heterogeneous photo-Fenton degradation of acid red B over Fe_2O_3 supported on activated carbon fiber. J. Hazard Mater. 285, 167–172.
Leary, R., Westwood, A., 2011. Carbonaceous nanomaterials for the enhancement of TiO_2 photocatalysis. Carbon 49, 741–772.
Li, Y., Zhang, F.S., 2010. Catalytic oxidation of Methyl Orange by an amorphous FeOOH catalyst developed from a high iron-containing fly ash. Chem. Eng. J. 158, 148–153.
Li, L., Zhou, G.M., Weng, Z., Shan, X.Y., Li, F., Cheng, H.M., 2014. Monolithic Fe_2O_3/graphene hybrid for highly efficient lithium storage and arsenic removal. Carbon 67, 500–507.
Ma, J.J., Zhou, L.C., Dan, W.F., Zhang, H., Shao, Y.M., Bao, C., Jing, L.Y., 2015. Novel magnetic porous carbon spheres derived from chelating resin as a heterogeneous Fenton catalyst for the removal of methylene blue from aqueous solution. J. Colloid Interface Sci. 446, 298–306.
Mazellier, P., Bolte, M., 2000. Heterogeneous light-induced transformation of 2,6-dimethylphenol in aqueous suspensions containing goethite. J. Photochem. Photobiol. Chem. 132, 129–135.
Meng, F.K., Li, J.T., Cushing, S.K., Bright, J., Zhi, M.J., Rowley, J.D., Hong, Z.L., Manivannan, A., Bristow, A.D., Wu, N.Q., 2013. Photocatalytic water oxidation by hematite/reduced graphene oxide composites. ACS Catal. 3, 746–751.
Navalon, S., Alvaro, M., Garcia, H., 2010. Heterogeneous Fenton catalysts based on clays, silicas and zeolites. Appl. Catal. B Environ. 99, 1–26.
Poulios, I., Micropoulou, E., Panou, R., Kostopoulou, E., 2003. Photooxidation of eosin Y in the presence of semiconducting oxides. Appl. Catal. B Environ. 41, 345–355.
Qiu, B.C., Xing, M.Y., Zhang, J.L., 2015. Stober-like method to synthesize ultralight, porous, stretchable Fe_2O_3/graphene aerogels for excellent performance in photo-Fenton reaction and electrochemical capacitors. J. Mater. Chem. 3, 12820–12827.
Rai, H.S., Bhattacharyya, M.S., Singh, J., Bansal, T.K., Vats, P., Banerjee, U.C., 2005. Removal of dyes from the effluent of textile and dyestuff manufacturing industry: a review of emerging techniques with reference to biological treatment. Crit. Rev. Environ. Sci. Technol. 35, 219–238.
Ruales-Lonfat, C., Barona, J.F., Sienkiewicz, A., Bensimon, M., Velez-Colmenares, J., Benitez, N., Pulgarin, C., 2015. Iron oxides semiconductors are efficients for solar water disinfection: a comparison with photo-Fenton processes at neutral pH. Appl. Catal. B Environ. 166, 497–508.
Shao, P.H., Tian, J.Y., Liu, B.R., Shi, W.X., Gao, S.S., Song, Y.L., Ling, M., Cui, F.Y., 2015. Morphology-tunable ultrafine metal oxide nanostructures uniformly grown on graphene and their applications in the photo-Fenton system. Nanoscale 7, 14254–14263.
Smith, B.A., Teel, A.L., Watts, R.J., 2004. Identification of the reactive oxygen species responsible for carbon tetrachloride degradation in modified Fenton's systems. Environ. Sci. Technol. 38, 5465–5469.
Song, H.J., Jia, X.H., Li, N., Yang, X.F., Tang, H., 2012. Synthesis of alpha-Fe_2O_3 nanorod/graphene oxide composites and their tribological properties. J. Mater. Chem. 22, 895–902.
Tian, J.Q., Li, H.Y., Xing, Z.C., Wang, L., Asiri, A.M., Al-Youbi, A.O., Sun, X.P., 2013. Facile synthesis of MWCNTs/Ag_3PO_4: novel photocatalysts with enhanced photocatalytic activity under visible light. J. Nanoparticle Res. 15, 1–7.
Tian, H., Fan, Y., Zhao, Y., Liu, L., 2014. Elimination of ibuprofen and its relative photo-induced toxicity by mesoporous BiOBr under simulated solar light irradiation. RSC Adv. 4, 13061–13070.
Vaughan, R.L., Reed, B.E., 2005. Modeling As(V) removal by a iron oxide impregnated activated carbon using the surface complexation approach. Water Res. 39, 1005–1014.
Vinothkannan, M., Karthikeyan, C., Kumar, G.G., Kim, A.R., Yoo, D.J., 2015. One-pot green synthesis of reduced graphene oxide (RGO)/Fe_3O_4 nanocomposites and its catalytic activity toward methylene blue dye degradation. Spectrochim. Acta Mol. Biomol. Spectrosc. 136, 256–264.
Wang, Q., Tian, S.L., Long, J., Ning, P., 2014. Use of Fe(II)Fe(III)-LDHs prepared by co-precipitation method in a heterogeneous-Fenton process for degradation of Methylene Blue. Catal. Today 224, 41–48.
Wassei, J.K., Kaner, R.B., 2013. Oh, the places you'll go with graphene. Acc. Chem. Res. 46, 2244–2253.
Williams, G., Seger, B., Kamat, P.V., 2008. TiO_2-graphene nanocomposites. UV-assisted photocatalytic reduction of graphene oxide. ACS Nano 2, 1487–1491.
Wu, P., Luo, X., Zhang, S., Li, K., Qi, F., 2015. Novel near room-temperature and/or light driven Fe-doped $Sr_2Bi_2O_5$ photo/thermocatalyst for methylene blue degradation. Appl. Catal. Gen. 497, 216–224.
Yang, X.L., Chen, W., Huang, J.F., Zhou, Y., Zhu, Y.H., Li, C.Z., 2015. Rapid degradation of methylene blue in a novel heterogeneous Fe_3O_4@rGO@TiO_2-catalyzed photo-Fenton system. Sci. Rep. 5, 10632–10641.
Yao, Y.J., Cai, Y.M., Lu, F., Qin, J.C., Wei, F.Y., Xu, C., Wang, S.B., 2014. Magnetic $ZnFe_2O_4$-C_3N_4 hybrid for photocatalytic degradation of aqueous organic pollutants by visible light. Ind. Eng. Chem. Res. 53, 17294–17302.
Yu, Z.Q., Chuang, S.S.C., 2007. Probing methylene blue photocatalytic degradation by adsorbed ethanol with in situ IR. J. Phys. Chem. C 111, 13813–13820.
Yu, X.J., Huang, L.Z., Wei, Y.C., Zhang, J., Zhao, Z.Z., Dai, W.Q., Yao, B.H., 2015. Controllable preparation, characterization and performance of Cu_2O thin film and photocatalytic degradation of methylene blue using response surface methodology. Mater. Res. Bull. 64, 410–417.
Yuan, B.L., Xu, J.G., Li, X.T., Fu, M.L., 2013. Preparation of Si-Al/alpha-FeOOH catalyst from an iron-containing waste and surface-catalytic oxidation of methylene blue at neutral pH value in the presence of H_2O_2. Chem. Eng. J. 226, 181–188.
Zaied, M., Peulon, S., Bellakhal, N., Desmazieres, B., Chausse, A., 2011. Studies of N-demethylation oxidative and degradation of methylene blue by thin layers of birnessite electrodeposited onto SnO_2. Appl. Catal. B Environ. 101, 441–450.
Zangeneh, H., Zinatizadeh, A.A.L., Habibi, M., Akia, M., Isa, M.H., 2015. Photocatalytic oxidation of organic dyes and pollutants in wastewater using different modified titanium dioxides: a comparative review. J. Ind. Eng. Chem. 26, 1–36.
Zhang, T.Y., Oyama, T., Horikoshi, S., Hidaka, H., Zhao, J.C., Serpone, N., 2002. Photocatalyzed N-demethylation and degradation of methylene blue in titania dispersions exposed to concentrated sunlight. Sol. Energy Mater. Sol. Cell. 73, 287–303.
Zhao, Y.C., Song, X.Y., Song, Q.S., Yin, Z.L., 2012. A facile route to the synthesis copper oxide/reduced graphene oxide nanocomposites and electrochemical detection of catechol organic pollutant. CrystEngComm 14, 6710–6719.
Zhou, B., Zhao, X., Liu, H.J., Qu, J.H., Huang, C.P., 2010a. Visible-light sensitive cobalt-doped $BiVO_4$ (Co-$BiVO_4$) photocatalytic composites for the degradation of methylene blue dye in dilute aqueous solutions. Appl. Catal. B Environ. 99, 214–221.
Zhou, X.M., Yang, H.C., Wang, C.X., Mao, X.B., Wang, Y.S., Yang, Y.L., Liu, G., 2010b. Visible light induced photocatalytic degradation rhodamine B on one-dimensional iron oxide particles. J. Phys. Chem. C 114, 17051–17061.